Computational Materials Science 71 (2013) 25–32

Contents lists available at SciVerse ScienceDirect

Computational Materials Science

journal homepage: www.elsevier.com/locate/commatsci

Simulations of anisotropic grain growth in single phase materials using Q-state Monte Carlo

J.B. Allen *, C.F. Cornwell, B.D. Devine, C.R. Welch

Information Technology Laboratory, U.S. Army Engineer Research and Development Center, Vicksburg, MS 39180, USA

ARTICLE INFO

Article history:
Received 7 September 2012
Received in revised form 19 November 2012
Accepted 14 January 2013
Available online 14 February 2013

Keywords:
Grain growth
Anisotropy
Q-state Monte Carlo
Computer simulation

ABSTRACT

The Q-state Monte Carlo, Potts model is used to investigate 2D, anisotropic, grain growth in single-phase materials using hexagonal grain elements. While many factors can affect the microstructure anisotropy, this research focusses on the role played by grain boundary energy anisotropy. Specifically, for each computed grain orientation and surface normal, the corresponding surface energy is assigned through a mapping process using Wulff plots. Various Wulff plot geometries are considered, and their respective impact on the grain growth anisotropy is evaluated. In addition to demonstrating the utility of this method for use with anisotropic grain growth models, this work advances the state of the art by providing a means of quantifying the degree of anisotropy through the use of statistics generated by frequency distributions of normalized grain radii.

Published by Elsevier B.V.

1. Introduction

Increased control of material microstructure, leading to enhanced mechanical and physical properties continues to be an active area of research. Occupying a central role in this research effort has been the ability to control grain growth. Numerous studies have demonstrated that a better understanding of grain growth processes is of fundamental importance in the fabrication of novel nanostructured materials. Several studies, for example, have shown that, as the average grain size of a material decreases, superior physical and mechanical properties can be achieved. For example, introducing nanocrystalline TiN into amorphous SiN_x, can result in hardness improvement of nanostructured Ti–Si–N films reaching maximum values of more than 40 GPa as the average size of TiN grains decreases to several tens of nanometers [1–3]. Further, by adding an amount of Al into TiN films, the solid solution (Ti1_xAlxN) formed has a substantially improved hardness and good thermal stability [4]. Other studies have emphasized the need to find ways of obtaining equiaxed, fine-grain microstructures without the occurrence of abnormal grain growth [5]. Issues relating to coarsening and shrinkage are of concern, as are the mechanisms which help to control the shape of grains.

Over the past few decades, a variety of analytical models have been proposed to predict grain growth kinetics [6,7]. These simplified analytical models, while helpful, do not simulate many of the vast complexities associated with grain growth kinetics. Computer simulations have in recent years become indispensable in exploring the details of grain growth and validating analytical models. Some of these computer models include: the phase field model [8], the Q-state Potts model [9], and the vertex model [10]. Among these, the Q-state Potts model has demonstrated the widest use among researchers, largely due to its relative simplicity to implement, its accuracy as evidenced by its validation record, and its robust extensibility to solve a vast number of problems involving microstructural evolution. Recently for example, the Q-state Potts model was extended to explore the grain growth mechanisms associated with various two-phase materials [2,11].

Most of these previous studies however, have been concerned with the processes associated with normal grain growth, wherein the average grain size increases while the shape of the size distribution remains constant with time. While this idealized simplification may be useful for simulating purely homogeneous materials (those without any secondary constituents), or for theoretical purposes, the majority of materials fall outside this idealized category and consist of varying degrees of anisotropic grain distributions. In fact, there is mounting evidence that suggests that certain material properties can be enhanced by deliberately introducing anisotropic grains within a fine-grained matrix. Faber and Evans [12,13] for example, found that anisotropic grain microstructures can result in increased fracture toughness of a material. Evidence for these findings came through observations of anisotropic grains responsible for crack deflection and bridging mechanisms in the crack wakes. Electrical and magnetic property enhancements have also been observed within anisotropic grain microstructures [14].

Grain anisotropy is a result of numerous factors, including: differences in grain boundary energy and mobility, segregation of

* Corresponding author. Address: 3909 Halls Ferry Road, Vicksburg, MS 39180-6199, USA. Tel.: +1 601 634 2335; fax: +1 601 634 2324.
E-mail address: Jeffrey.B.Allen@erdc.dren.mil (J.B. Allen).

0927-0256/$ - see front matter Published by Elsevier B.V.
http://dx.doi.org/10.1016/j.commatsci.2013.01.022

solutes on different boundaries [5], the presence of an amorphous liquid phase [15], interface growth velocity differences during phase transformation [16] and the anisotropy of the interfacial energy between two phases [17,18]. Unfortunately, there is little understanding about how these factors affect the evolution of an anisotropic microstructure. It is well known that the driving force for grain growth is the reduction in the total grain boundary energy, achievable by reducing the total grain boundary area of a system. Therefore, it is natural to assume that one of the most important factors for controlling anisotropic grain growth is the grain boundary energy anisotropy.

This work may be regarded as a continuation of the work conducted by Yang et al. [5] involving the effect of grain boundary energy anisotropy on anisotropic grain growth. Proceeding therefore in a similar manner, a Q-state Monte Carlo, Potts model is developed to investigate 2D, anisotropic grain growth in single-phase materials. While many factors can affect the microstructure anisotropy, this research focusses on the role played by grain boundary energy anisotropy, which will be assigned via the use of Wulff plots. Specifically, for each computed grain orientation and surface normal, the corresponding surface energy will be assigned through a mapping process involving various polar Wulff plot configurations. For each configuration, the impact on the grain growth anisotropy will be evaluated. In addition to demonstrating the utility of the Q-state Monte Carlo method for use with anisotropic grain growth models, this work serves to advance the state of the art by providing a means of quantifying the degree of anisotropy through the use of statistics generated by frequency distributions of normalized grain radii. A practical application of this model would be to produce prescribed anisotropic polycrystalline ceramic structures through the purposeful orientation of the crystalline grains in the green form, and then use the model's predictive capabilities to engineer the sintering process to facilitate anisotropic grain growth.

2. The model

A two dimensional lattice of cells (100×100) representing the initial grain microstructure was created and initialized by randomly assigning an integer number q_i between 1 and Q to each lattice site (i). Here Q is the total number of degenerate spins (grain orientations) within the system and was initialized with random integers between 1 and 60. Although in reality there are a continuous range of possible orientations, previous research has shown that for sufficiently large values of Q (i.e., $Q > 50$) the results may be assumed independent of initial orientation number [9]. The cell resolution (100×100) was deemed sufficient based on the results of a benchmark, isotropic test case, which compared favorably (at this resolution) with analytical results based on a power law kinetics model [9,19,20]. Further, hexagonal elements (see Fig. 1) were selected for this work rather than rectangular elements, since the latter has been known to cause inaccurate results due to the effects of lattice pinning [21,22].

In accordance with the model used by Yang et al. [5], the interaction energy between two neighboring cells $E_\theta(q_1, q_2)$ can be expressed as:

$$E_\theta(q_1, q_2) = (1 - \delta_{q_1 q_2})\{J_\theta(q_1) + J_\theta(q_2) - J_b\} \tag{1}$$

where $\delta_{q_1 q_2}$ is the Kronecker delta function ($\delta_{q_1 q_2} = 1$ if $q_1 = q_2$; and $\delta_{q_1 q_2} = 0$ if $q_1 \neq q_2$), $J_\theta(q_i)$ is the surface energy of a cell with state q_i along a surface normal, defined by the direction θ (where $\theta = 0$, $\pi/3$, or $2\pi/3$), and J_b is the grain boundary binding energy. Applying the Kronecker delta function, Eq. (1) may be expressed more conveniently as:

$$E_\theta(q_1, q_2) = \begin{cases} 0 & \text{if } q_1 = q_2 \\ J_\theta(q_1) + J_\theta(q_2) - J_b & \text{if } q_1 \neq q_2 \end{cases} \tag{2}$$

The total system energy over all nearest-neighbors is thus given by the Hamiltonian:

$$E_{tot} = \frac{1}{2}\sum_{q_1}\sum_{q_2} E_\theta(q_1, q_2) \tag{3}$$

Grain growth is simulated using the method developed in several previous works [23–25]. To summarize, first a lattice site is chosen at random from the simulation space. Then a new state q is chosen at random from the Q possible states of the system. The change in energy (ΔE) is computed using Eq. (3) and the probability (P) that the site will change orientation is then determined from the transition probability function:

$$P = \begin{cases} M \exp\left(-\frac{\Delta E}{k_B \tau}\right) & \Delta E > 0 \\ M & \Delta E \leqslant 0 \end{cases} \tag{4}$$

where ΔE is the change in energy associated with the reorientation event, k_B is the Boltzmann constant, M is the grain boundary mobility, and τ is simulation temperature.

The method for determining the surface energies $J_\theta(q_i)$ where $\theta = 0$, $\pi/3$, or $2\pi/3$ closely follows that of [5]. For purposes of completeness we summarize the procedure here. The orientation angle (φ) for a given hexagonal cell is computed as $\varphi = \pi q/Q$, where q is any one of the Q integer orientations. This angle is then mapped to a Wulff plot (a polar plot described by the surface orientation angle and radii composed of surface energies), wherein φ is used to locate the position of the surface orientation energy (γ_1) located at

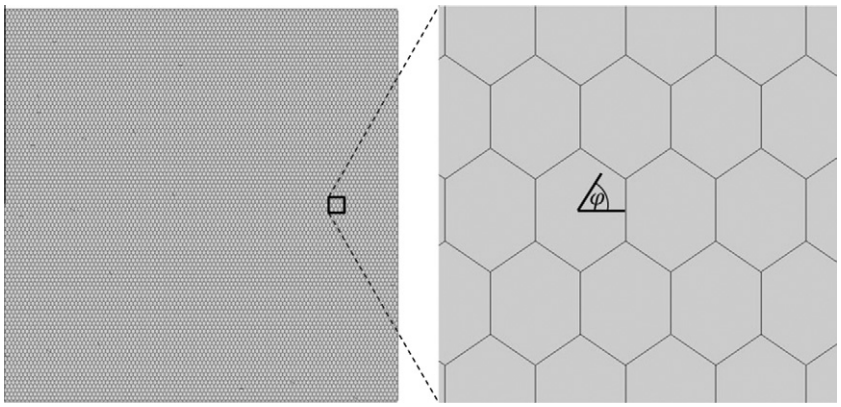

Fig. 1. Hexagonal grain elements and definition of orientation angle (φ).

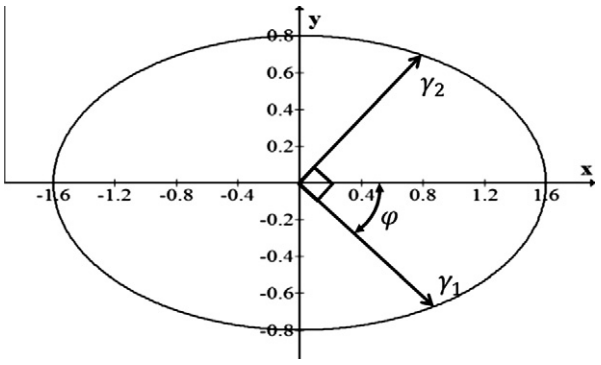

Fig. 2. Elliptical ($n = 2$) Wulff plot with surface energy determination.

an angle φ from the x-axis (see Fig. 2). Due to the twofold rotational symmetry of the Wulff plot, the surface energy of surface two (γ_2) is located along a surface orientation vector that is 90° from surface one, while γ_3 is equal to the minimum of γ_1 and γ_2. In this way, grains with orientation number from 1 to $Q/3$ have higher surface energies along the $\theta = 0$ direction than the other two directions; grains with orientation number from $Q/3 + 1$ to $2Q/3$ have higher surface energies along the $\theta = \pi/3$ orientation; and grains with orientation number from $2Q/3 + 1$ to Q have higher surface energies along the $\theta = 2\pi/3$ direction. For implementation purposes, the following algorithm describes the process used in this study:

$$\text{if } 1 \leqslant \varphi \leqslant \frac{Q}{3} \text{ then } J_{\theta=0}(q_i) = \gamma_1; \quad \gamma_2 = \gamma_{1+\pi/2}; \quad \gamma_3 = \min(\gamma_1, \gamma_2)$$

$$\text{else if } \frac{Q}{3} + 1 \leqslant \varphi \leqslant \frac{2Q}{3} \text{ then } J_{\theta=\pi/3}(q_i) = \gamma_1; \quad \gamma_2 = \gamma_{1+\pi/2}; \quad \gamma_3 = \min(\gamma_1, \gamma_2)$$

$$\text{else if } \frac{2Q}{3} + 1 \leqslant \varphi \leqslant Q \text{ then } J_{\theta=2\pi/3}(q_i) = \gamma_1; \quad \gamma_2 = \gamma_{1+\pi/2}; \quad \gamma_3 = \min(\gamma_1, \gamma_2)$$

For this study, various Wulff plot configurations were used, each based on the equation for a "super-ellipse" (or Lamé curve), which may be represented in rectangular coordinates as:

$$\left|\frac{x}{a}\right|^n + \left|\frac{y}{b}\right|^n = 1 \tag{5}$$

where a and b are positive, real numbers corresponding to the semi-major and semi-minor axes, respectively, and n is a positive real number describing the shape of the curve. In polar coordinates (r, θ) Eq. (5) may be written as:

$$r(\theta) = \left(\left|\frac{\cos(\theta)}{a}\right|^n + \left|\frac{\sin(\theta)}{b}\right|^n\right)^{-1/n} \tag{6}$$

Fig. 3 shows the graphical results of Eq. (6), for four simulated super-ellipses, each with a different value of n. Yang et al. [5] found that in order to develop highly anisotropic grain structures, the Wulff plot must have a maximum surface energy along one

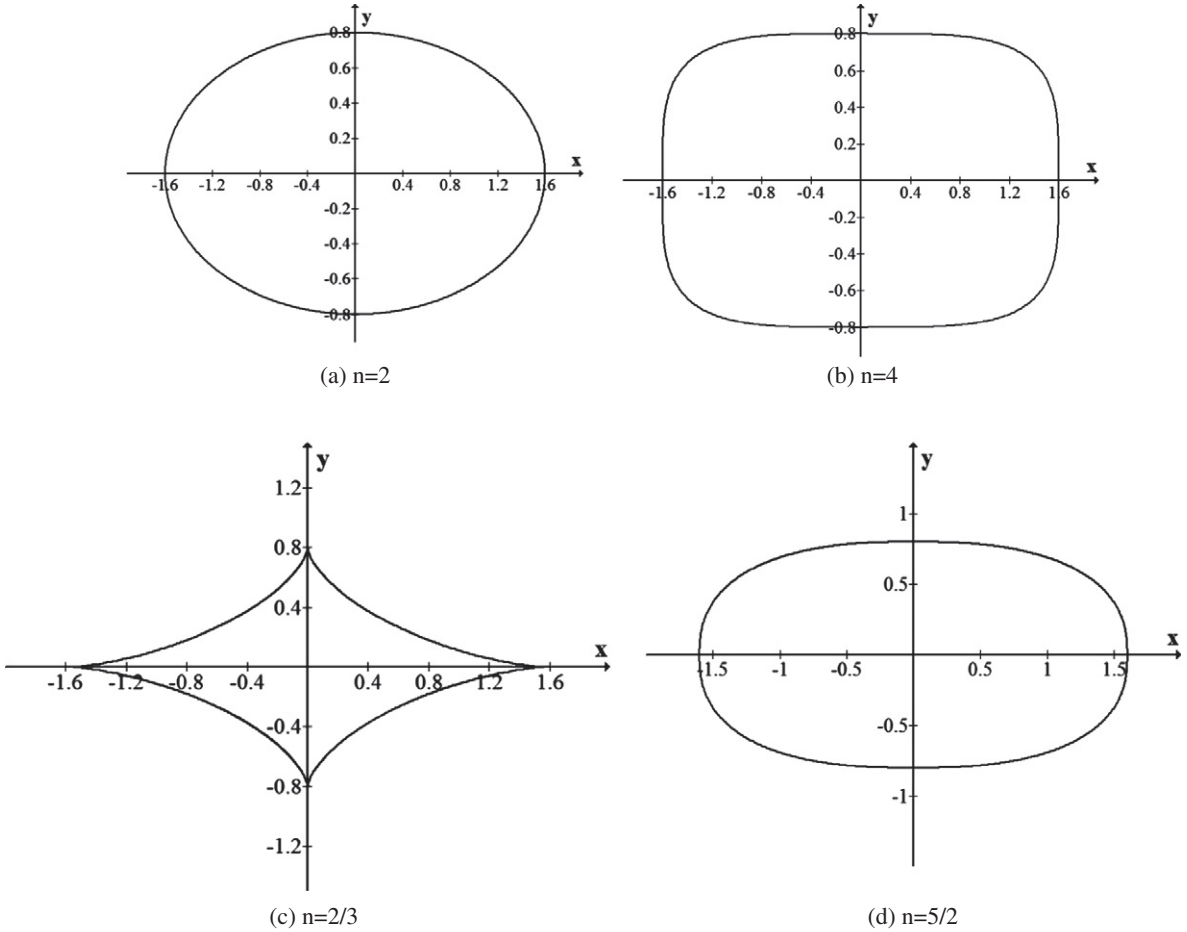

Fig. 3. Elliptical Wulff plot geometries used in this study.

semi-major axis and a minimum surface energy along the other. Therefore throughout this work, for purposes of simplification, we have selected constant semi-major and semi-minor axis values of $a = 1.6$ and $b = 0.8$, respectively.

The hexagonal grid was developed using the GAMBIT grid generation tool [26], and the anisotropic Monte-Carlo algorithm was developed within OpenFOAM [27]. While traditionally used for solving Computational Fluid Dynamics (CFD) problems, OpenFOAM was selected for this work due to its existing cell-to-cell communication algorithms and parameter passing capabilities. For each of the four computer simulations, including one isotropic validation case (consisting of a circular Wulff plot), the microstructure was represented using an array of 100×100 hexagonal elements. The simulations were run serially using a 64 bit, Intel Xeon processor running at 1.86 GHz. The use of periodic boundary conditions was applied along all domain boundaries, the grain boundary binding energy was fixed at a constant value of 0.3, and the number of allowed initial grain orientations (Q) was 60. As customary, the simulation time was measured in Monte Carlo steps, wherein one Monte Carlo Step was equivalent to 100×100 reorientation attempts. A simulation temperature of $k_B\tau = 0$ was used throughout, and selected for its favorable ability to simulate grain growth phenomenon [25]. Note that the simulation temperature is not an actual physical temperature. Indeed setting $\tau = 0$ does not eliminate grain growth but merely eliminates thermal fluctuations and ensures the rejection of all steps for which $\Delta E > 0$ The effects due to actual temperatures are included within the grain boundary mobility (M), which is related to the actual temperature (T) via the Arrhenius equation:

$$M = M_0 \exp\left(\frac{-Q}{k_B T}\right) \tag{7}$$

where Q is the activation energy for grain boundary migration and M_0 is the usual Arrhenius prefactor. Although in future studies we may wish to evaluate the effects due to temperature variation, for this study we have assumed a constant temperature throughout the simulation domain and assigned a constant value of one for the grain boundary mobility. For post-processing purposes, the average grain size was computed according to:

$$\langle R\rangle = \frac{\sum_i^N n_i R_i}{\sum_i^N n_i} \tag{8}$$

where N is the total number of grains, and n_i is the number of grains of size R_i.

3. Results

For reference purposes, the model was first calibrated for isotropic grain boundary energies, that is, for surface energies which are assumed independent of grain orientation. In this case, the semi-major and minor axes of the Wulff plot are identical, and a circle is produced. The microstructure evolution is shown in Fig. 4 over four time periods, ranging from time $t = 0$ MCS to $t = 4000$ MCS, where one Monte Carlo Step (MCS) is equivalent to 100×100 reorientation attempts. As indicated, after 4000 MCS only about 100 grains remain, all with approximately equivalent aspect ratios which is a characteristic feature of isotropic grain growth. The disappearance of grains over time is due to the reduction of total grain boundary energy and occurs by reducing the total grain boundary area of the system.

The evolution of the average grain size $\langle R\rangle$ can be described by power-law kinetics [9,19,20]:

$$\langle R\rangle = \alpha t^{1/r} \tag{9}$$

where α is a constant dependent on temperature, t is the time (in MCS units), and r is the grain growth exponent. For single phase systems, a grain growth exponent of 0.5 has been confirmed experimentally [9,28]. The slope of a straight fit through a plot of $\log\langle R\rangle$ vs. $\log(t)$ by least squares fitting gives the inverse of the grain growth exponent ($1/n$). As shown in Fig. 5, to a good approximation, the slope (0.49) is in agreement with the power law prediction.

The microstructure evolution corresponding to anisotropic grain growth (ellipse; $n = 2$) is shown in Fig. 6, and corresponds to 0, 100, 1000, and 4000 MCS. Unlike the isotropic grain growth model, the energy of a grain boundary is not constant, but a function of the orientations of grains on all sides of the grain boundary. Anisotropic grains result from the non-equilibrium effect of high energy grain boundaries which tend to migrate faster than corresponding low energy boundaries. Occasionally, neighboring grains will have equivalent (or near equivalent) surface energies, which results in some of the grains remaining isotropic.

As indicated, at time $t = 0$ MCS (Fig. 6a), the grains appear fully isotropic (low aspect ratios), maintain a narrow size distribution, and cover the full range of orientation states. In this initial stage, the grain growth is primarily driven by grain boundary curvature. As shown, the initial grain states conform to a random distribution. At time $t = 100$ MCS (Fig. 6b), the isotropic growth tendency is maintained for all but a small subset of grains, which show early tendencies toward anisotropy, indicating elongated growth along directions corresponding to the grain surface normal (0°, 60°, and 120°). At time $t = 1000$ MCS (Fig. 6c), the number of isotropic grains have been reduced significantly. This is due to the higher grain boundary energies associated with the anisotropic grains, and the resultant increase in growth rate of these elongated grains. The consumption of the isotropic grains is a direct result of this process. Finally, at time $t = 4000$ MCS (Fig. 6d), there are only a few isotropic grains remaining. The average grain size has more than quadrupled, and the number of original grain orientations (states) has been reduced significantly.

Fig. 7 shows the microstructure results at time $t = 4000$ MCS corresponding to four different Wulff plots with $n = 2$, $n = 4$, $n = 2/3$, and $n = 5/2$. As indicated, each plot shows marked differences from the isotropic results shown in Fig. 4, including grains having clear, directional growth preferences and rectangular dimensions with relatively high aspect ratios. Upon closer inspection, the $n = 2$ and $n = 5/2$ microstructures (Fig. 7a and d) appear quite similar in a variety of ways, including, grain number, average grain size, grain aspect ratio, and grain orientation distribution. The $n = 4$, and $n = 2/3$ plots (Fig. 7b and c), in contrast appear to contain a fair number of abnormal grains, easily distinguishable by the significant disparity in grain size between the largest and smallest grains. The $n = 4$ plot (Fig. 7b) is additionally unique, in that a much smaller subset of the original grain orientations remain than in any of the other three cases.

Fig. 8 shows a plot of the average grain size over time for each of the four Wulff plot configurations. As indicated, the $n = 2$ and $n = 5/2$ configurations exhibit a decreased tendency toward average grain growth after approximately 2000 MCS, with an average grain size of $\langle R\rangle = 5$. In contrast, the $n = 4$ and $n = 2/3$ configurations show a steady increase in grain size with an approximately linear upward slope of 0.001. As previously shown in Fig. 7, this latter trend is due to the increased amount of abnormal grain growth, which increasingly favors the abnormally large grains in order to reduce the total system energy.

Fig. 9 shows the frequency distribution of the normalized grain size ($R/\langle R\rangle$) for each of the four Wulff plot configurations shown in Fig. 3, as well as the isotropic case (corresponding to a circular Wulff plot). For each case, the simulations ran for a total of 4000 MCS. The normalized grain size was separated into 30 groups between 0 and 3, and the frequency was defined as the ratio of the

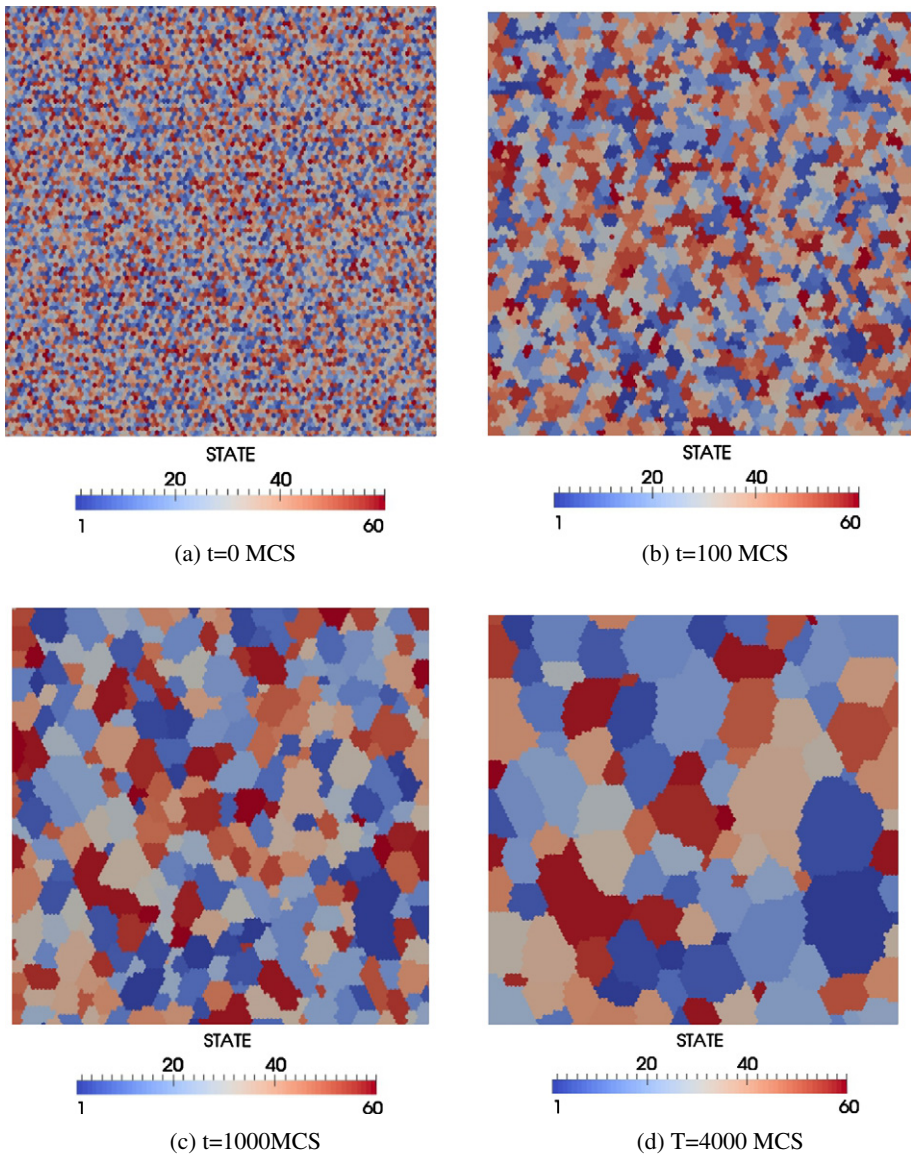

Fig. 4. Isotropic grain growth; 100 × 100 hexagonal elements; circular Wulff plot ($a = 1.0$, $b = 1.0$, $n = 2$); $Q = 60$.

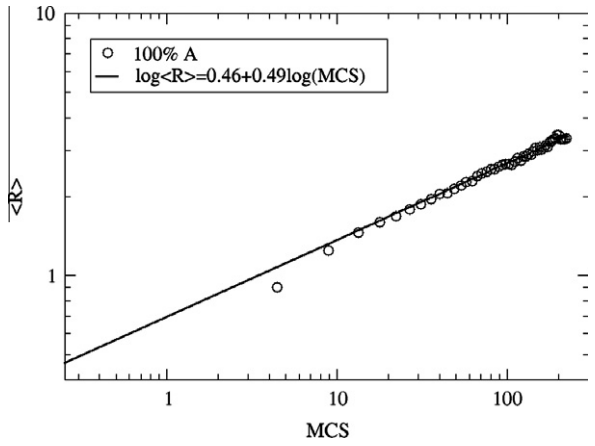

Fig. 5. The slope of a straight fit through a plot of $\log\langle R\rangle$ vs. $\log(t)$ by least squares fitting provides an estimate for the grain growth exponent $(1/n)$. As shown, to a good approximation, the slope (0.49) is in agreement with the power law prediction.

number of grains within one group divided by the total number of grains.

As expected, each case is represented by a log-normal distribution with positive skew, and is easily distinguishable from its neighbor distributions by comparing values of mean ($\mu_{R/\langle R\rangle}$), standard deviation ($\sigma_{R/\langle R\rangle}$), and skewness (see Table 1). Here the degree of skewness (a measure of data symmetry) is represented as:

$$Skewness = \frac{\sum_{i=1}^{N}((R/\langle R\rangle)_i - \mu_{R/\langle R\rangle})^3}{(N-1)\sigma_{R/\langle R\rangle}} \tag{10}$$

where N is the total number of grains (for MCS = 4000), and $(R/\langle R\rangle)_i$ is the normalized grain size for grain i.

As indicated, the isotropic case is represented by a log-normal distribution with a mean normalized grain radius of approximately one, a standard deviation 0.54, and a skewness of 0.84. In contrast, each of the elliptical distributions shows average grain radii significantly less than one and skewness values, in some cases greater than two. As shown, the $n = 2$ and $n = 5/2$ elliptical distributions have nearly equivalent mean radii of 0.66, and 0.67, respectively, but show significant disparity with respect to both the standard deviation and skewness values. The $n = 4$ and $n = 2/3$ elliptical

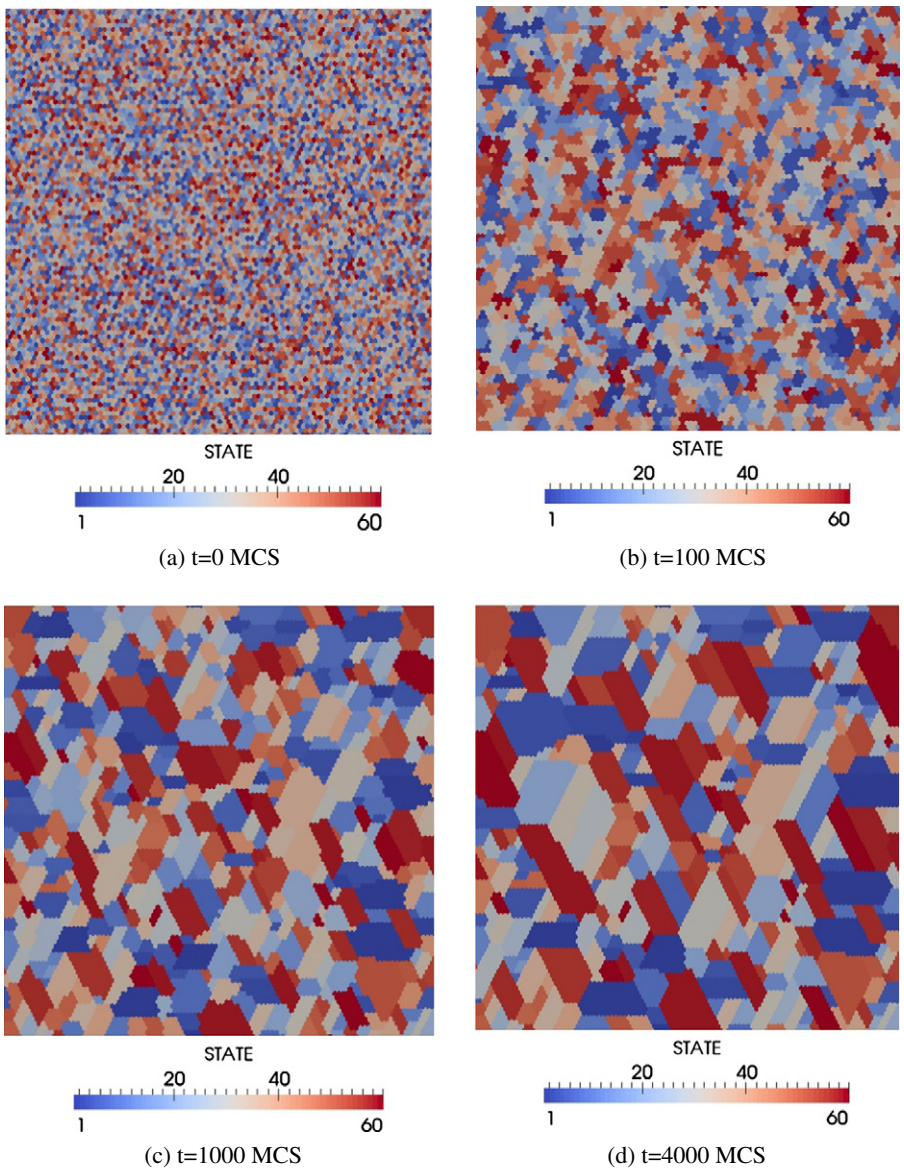

Fig. 6. Anisotropic grain growth; 100 × 100 hexagonal elements; ellipsoid Wulff plot ($a = 1.6$, $b = 0.8$, $n = 2$); $Q = 60$.

distributions also have nearly equivalent mean radii (0.85), but unlike the $n = 2$ and $n = 5/2$ cases, show similar values for skewness. Table 1 also shows the total number of grains (N) that remained at time $t = 4000$ MCS. As shown, the isotropic case resulted in the coarsest microstructure ($N = 176$), while the elliptical distributions maintained grain numbers in correlation to their previous statistical similarities. That is, the $n = 2$ and $n = 5/2$ distributions averaged grain numbers close to 400, while the $n = 4$ and $n = 2/3$ distributions averaged approximately 200 grains.

Clearly these results serve to confirm the qualitative results observed in Fig. 7. The abnormal grain growth seen for the $n = 4$ and $n = 2/3$ configurations are characterized by a disproportionately high number of unusually large grains which tend to consume smaller grains. It well understood that this naturally occurs in order to reduce the total grain boundary surface area and thus the total system energy. Less certain, is why this abnormal grain growth occurs for these two Wulff plot configurations and not for the $n = 2$ and $n = 5/2$ cases. Referring to Fig. 3, one possible explanation may be due to the fact that the $n = 4$ elliptical configuration shows maximum grain boundary surface energies lying not along a primary axis (as in the case of the $n = 2$ and $n = 5/2$ cases) but along intermediate x–y locations. Similarly, the $n = 2/3$ configuration shows minimum grain boundary energies not along the y-axis but again along intermediate x–y locations. The excess of energy (in the $n = 4$ case) or the lack of energy (in the $n = 2/3$ case) along these intermediate locations likely contributes to the occurrence of the observed abnormal grain growth.

4. Practical application for the model

A practical application of the model is to allow prescribed anisotropic polycrystalline ceramic structures to be synthesized. As mentioned previously, such structures may provide increased fracture toughness [12,13] among other attributes. Key to the process would be to purposely orient crystalline grain structure in the green form. Such orientation might be achieved by depositing ions or iron particles on preferred faces of the grains, and then applying electric or magnetic fields combined with vibration to orient the grains along prescribed axes. The model's predictive capabilities could then be used to engineer the sintering process to cause anisotropic grain growth.

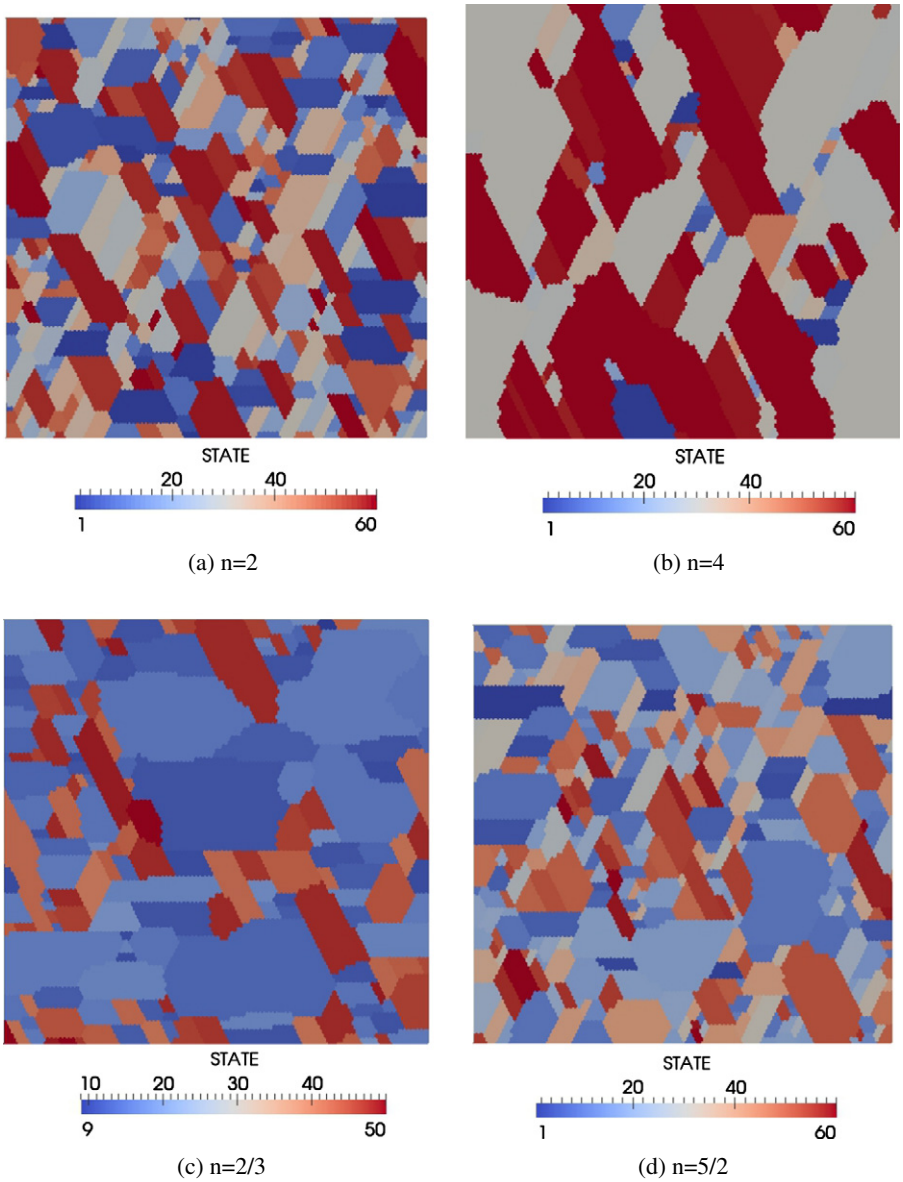

Fig. 7. Anisotropic grain growth; 100 × 100 hexagonal elements; ellipsoid Wulff plots ($a = 1.6$, $b = 0.8$) corresponding to $n = 2$, $n = 4$, $n = 2/3$, and $n = 5/2$; $Q = 60$; $t = 4000$ MCS.

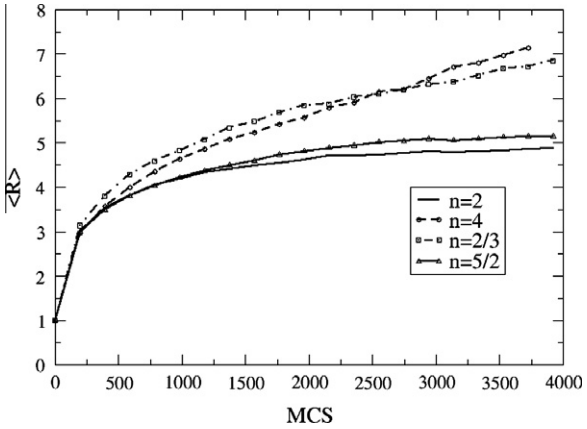

Fig. 8. Average grain size $\langle R \rangle$ vs. simulation time (MCS) for Wulff plot geometries: $n = 2$, $n = 4$, $n = 2/3$, and $n = 5/2$.

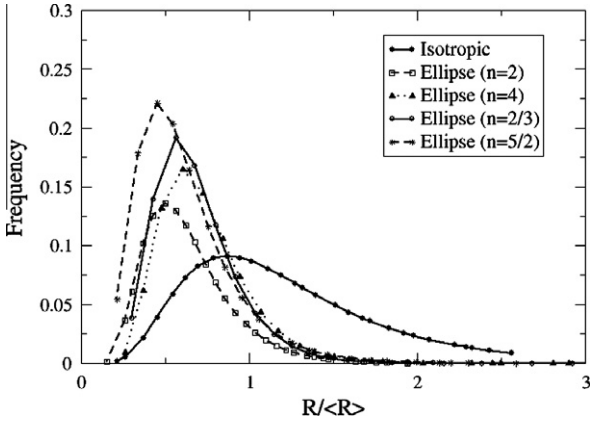

Fig. 9. Normalized grain size distributions corresponding to the isotropic and elliptical Wulff plots ($n = 2$, $n = 4$, $n = 2/3$, and $n = 5/2$) at $t = 4000$ MCS.

Table 1
Grain size distribution statistics corresponding to the isotropic and elliptical Wulff plots ($n = 2$, $n = 4$, $n = 2/3$, and $n = 5/2$) at $t = 4000$ MCS.

Case	$\mu_{R/\langle R\rangle}$	$\sigma_{R/\langle R\rangle}$	Skewness	Total grain num. (N)
Isotropic ($a = b = 1$)	0.99	0.54	0.84	176
Elliptical ($a = 1.6$; $b = 0.8$; $n = 2$)	0.66	0.32	1.30	412
Elliptical ($a = 1.6$; $b = 0.8$; $n = 4$)	0.85	0.65	1.90	194
Elliptical ($a = 1.6$; $b = 0.8$; $n = 2/3$)	0.85	0.58	2.01	209
Elliptical ($a = 1.6$; $b = 0.8$; $n = 5/2$)	0.67	0.40	2.08	371

5. Conclusions

The Q-state Monte Carlo, Potts model was used to investigate 2D, anisotropic, grain growth in single-phase materials. While many factors can affect the microstructure anisotropy, this research focused on the role played by the grain boundary energy. Hexagonal grain elements were used in order to avoid the dependence of grain growth kinetics on the lattice geometry and various Wulff plot configurations were used in order to map surface energies to the lattice geometry. From this research, the following conclusions may be drawn:

(1) The Q-state Monte Carlo method provides an efficient and reliable means for the characterization of single phase grain growth studies.
(2) The shape of the Wulff plot, as governed by the values for the semi-major and semi-minor axes, as well as the exponential factor (n), plays a critical role in the resulting microstructure.
(3) Isotropic grains were shown to exhibit equiaxed growth due to equivalent surface energies of neighboring grains.
(4) Anisotropic grains resulted from the non-equilibrium effect of high energy grain boundaries which tended to migrate faster than corresponding low energy boundaries.
(5) Abnormal, anisotropic grain growth may be encountered for certain elliptical Wulff plot configurations (i.e., $n = 4$, and $n = 5/2$), and were characterized by a disproportionately high number of unusually large grains which tended to consume the smaller grains.
(6) Compared to isotropic grain growth, anisotropic grain growth may be characterized by lognormal grain size distributions with smaller average grain sizes and relatively large skewness values.
(7) The model provides a method to engineer the sintering process to enhance material properties by deliberately introducing anisotropic grain orientation within green form prior to sintering to achieve the desired anisotropic polycrystalline ceramic structures in the final product.

Future studies will be conducted in order to examine the role of various other factors affecting anisotropic grain growth, including the application of temperature gradients, the extension to three dimensions, and the addition of second phase materials.

Acknowledgments

This study was funded through the U.S. Army Engineer Research and Development Center Directed Research Programs: "Nanoscale Studies of Polycrystalline Materials with Emphasis on Ceramics Synthesis" and "Effects of Grain Boundaries on Ceramic Properties" as part of the Advanced Material Initiative program.

References

[1] S.C. Tjong, H. Chen, Mater. Sci. Eng. R 45 (2004) 1.
[2] Z.J. Liu, C.H. Zhang, Y.G. Shen, Y.-W. Mai, J. Appl. Phys. 95 (2004) 758.
[3] C. Lu, Y.-W. Mai, Y.G. Shen, J. Mater. Sci. 41 (2006) 937.
[4] Z.-J. Liu, P.W. Shum, Y.G. Shen, Thin Solid Films 468 (2004) 161.
[5] W. Yang, L. Chen, G. Messing, Mater. Sci. Eng. A195 (1995) 179.
[6] I.M. Lifshitz, V.V. Slyozov, J. Phys. Chem. Solids 19 (1961) 35.
[7] M. Hillert, Acta Metall. 13 (1965) 227.
[8] D. Fan, L.-Q. Chen, Acta Mater. 45 (1997) 3297.
[9] M.P. Anderson, D.J. Srolovitz, G.S. Grest, P.S. Sahni, Acta Metall. 32 (1984) 783.
[10] J. Baxter, Exactly Solved Models in Statistical Mechanics, Academic Press, London, 1982.
[11] Y.G. Zheng, C. Lu, Y.-W. Mai, Y.X. Gu, H.W. Zhang, Z. Chen, Appl. Phys. Lett. 88 (2006) 144103.
[12] K.T. Faber, A.G. Evans, M.D. Drory, Fract. Mech. Ceram. 6 (1983) 77.
[13] K.T. Faber, A.G. Evans, Acta Metall. 31 (1983) (1983) 565.
[14] L.T. Bowen, EJ. Avella, J. Appl. Phys. 54 (1983) 2764.
[15] W.A. Kaysser, M. Sprissler, C.A. Handwerker, J.E. Blendell, J. Am. Ceram. Soc. 70 (1987) 339.
[16] O. Ito, E.R. Fuller Jr., Acta Metall. Mater. 41 (1992) 191.
[17] A.H. Heuer, G.A. Fryburg, L.U. Ogbuji, T.E. Mitchell, S. Shinozaki, J. Am. Ceram. Soc. 61 (1978) 406.
[18] T.E. Mitchell, L.U. Ogbuji, A.H. Heuer, J. Am. Ceram. Soc. 61 (1978) 412.
[19] M.A. Fortes, Materials Science Forum, vol. 94, Trans Tech. Publications, Switzerland, 1992.
[20] S.K. Kurtz, F.M.A. Carpay, J. Appl. Phys. 51 (1980) 5725.
[21] E.A. Holm et al., Phys. Rev. A 43 (1991) 2662.
[22] E.A. Holm, D.J. Srolovitz, J.W. Cahn, Acta Metall. Mater. 41 (1993) 1119.
[23] D.J. Srolovitz, G.S. Grest, M.P. Anderson, A.D. Rollett, Acta Metall. 36 (1988) 2115.
[24] J. Wejche, D. Weaire, J.P. Kermode, Phil. Msg. B53 (1986) 15.
[25] E.A. Holm, J.A. Glazier, D.J. Srolovitz, G.S. Grest, Phys. Rev. A 43 (1991) 2662.
[26] Gambit Users Guide, Lebanon, NH, 2007.
[27] OpenFoam, The Mews, Picketts Lodge, Surrey RH1 5RG, UK, 2006.
[28] H.V. Atkinson, Acta Metall. 36 (1988) 469.